JAAS FULL PAPER
www.rsc.org/jaas

Characteristics of atomic absorption calibration curves with the transversely heated graphite furnace

László Bencs,*[a]† Ottó Szakács,[b] Norbert Szoboszlai,[c] Zsolt Ajtony[d] and Gábor Bozsai[e]

[a]*Micro and Trace Analysis Centre, University of Antwerp, Universiteitsplein 1, B-2610 Antwerp, Belgium*
[b]*Research Institute for Solid State Physics and Optics, Hungarian Academy of Sciences, PO Box 49, H-1525 Budapest, Hungary*
[c]*Department of Inorganic and Analytical Chemistry, Loránd Eötvös University of Sciences, PO Box 32, H-1518 Budapest, Hungary*
[d]*Institute of Food Science, University of West Hungary, H-9200 Mosonmagyaróvár, Lucsony u. 15-17, Hungary*
[e]*Central Chemical Laboratory, József Fodor National Public Health Center, PO Box 22, H-1450 Budapest, Hungary*

Received 21st August 2002, Accepted 3rd December 2002
First published as an Advance Article on the web 14th January 2003

Calibration curves with two quasi-linear sections (''double sloping'') were observed for the medium volatile elements, Cr and Cu, with the use of a SIMAA 6000 graphite furnace atomic absorption spectrometer under interrupted internal gas flow conditions. If a standard transversally heated graphite atomizer (THGA) tube was shortened by 0.5 mm at both of its ends, (*i.e.* the gaps were enlarged between graphite furnace housing and tube ends), a stronger declination of the calibration curves resulted. Elements with fairly high diffusion coefficients (>5.8 cm^2 s^{-1}) and with short appearance time of their transients (<0.6 s), such as Cr and Cu, have shown the most characteristic sensitivity drop towards higher concentrations. This anomalous feature could be eliminated in three different ways; (1) by applying end-capped THGA tubes, (2) using mini-flow (50 cm^3 min^{-1}) conditions during the atomization stage, and (3) by adding Pd–Mg chemical modifier. For the low volatile Mo and V, the calibration curves had no irregular shape. For Ag, Co, Cr, Cu, Mn and Ni, the mini-flow settings improved the linearity of the calibration curves and extended the upper limit of the linear calibration range by a factor of 1.5–2.0. The irregular characteristic of the analytical curves was interpreted as an increased vapour loss at higher analyte concentrations through the opened ends of the standard THGA tubes. This vapour loss was associated with the significantly diverse expulsion velocities of atoms, caused by the difference in temperature and concentration gradients, when evaporating amounts of analytes with more than one order of magnitude difference.

Introduction

In previous studies, graphite furnace atomic absorption spectrometry (GFAAS) methods were elaborated to determine some dopants in bismuth tellurite (Bi_2TeO_5) optical crystals,[1–5] partly, with the use of a SIMAA 6000 spectrometer. This GFAAS system, incorporating the Stabilized Temperature Platform Furnace concept,[6] is equipped with a transversely heated graphite tube atomizer (THGA) fitted with longitudinal Zeeman-effect background (BG) corrector, and an echelle polychromator optics with a charge coupled device detector, exhibiting the simultaneous, multi-element determination of up to six analytes.[7,8]

An earlier application of the SIMAA 6000 spectrometer with fast furnace programs resulted in linear calibration curves for the medium volatile Co and Cu.[9] On the other hand, the calibration curves were made up of two linear sections of different slopes for the high volatile Cd and Pb. The characteristic mass (m_0) values for the upper parts of the analytical curves were similar to those specified by the manufacturer. However, in the lower concentration range, enhanced m_0 values were found for both elements. Hoenig and Cilissen[9] explained this deviation with an increased diffusional loss of sample vapours from standard THGA tubes at higher analyte amounts. They also offered an alternative explanation for the irregular calibration curves,[9] attributing them to a heterogeneous spatial distribution of atoms in the furnace combined with an uneven distribution of the radiation from the primary radiation source.[10,11] To eliminate the vapour loss and the irregularity of the calibration, the application of end-capped THGAs (*i.e.* tubes with cylindrical restrictions at their ends) was suggested.[9]

The first transversely heated furnace, called Integrated Contact Cuvette (ICC), was developed by Frech *et al.*[12] In the THGA furnace, similarly to the ICC design, the L'vov concept of an ''ideal atomizer'' prevailed, *i.e.* the sample vapours could enter into an analytical zone of higher and constant temperature.[13] This feature was experimentally proven by Sperling *et al.*[14] Conversely, even in the advanced THGA furnaces, the condensation of analytes in the presence of microgram masses of matrix vapours can be effective in the regions of colder tube ends, resulting in a decreased absorbance signal.[15] This drawback could be circumvented by the use of end-capped tubes,[15] which design has several analytical advantages over the standard THGA tubes; *e.g.* the lower limit of detection (LOD).[16–18]

The removal mechanisms of sample vapours in THGA furnaces were distinguished as (a) concentration diffusion, (b) natural convection, and (c) forced convection.[16,19] Improvement of the atomizer housing helped to minimize the natural convective flows,[19] but unchanged the magnitude of matrix effects,[20] which is true for the rest removal mechanisms. Pilot studies on the distribution of atomic vapour[21] revealed that the density of Rb atoms 1.2 mm outside of the THGA tube end was

†Present address: Research Institute for Solid State Physics and Optics, Hungarian Academy of Sciences. E-mail: bencs@szfki.hu

14% of that at the centre of the standard tubes, while for the end-capped tubes it was 17%. The Rb atoms outside of the tube accounted for about 6% of the total signal for both tube types.[21]

Gilmutdinov *et al.*[22] pointed out that the spatial non-uniformity of the absorbing layer affected the concentration curves much more strongly than the spectral features of the analytical lines. The longitudinal temperature and concentration gradients resulted in a decrease of the slope of the concentration curves, while the cross-section non-uniformities led to the curvature of the concentration curves.[22]

In the present work, the shape of the calibration curves for some analytes of medium, and low volatility are studied with the use of the SIMAA 6000 spectrometer. The effects of four sets of the atomization conditions were studied; (1) use of end-capped graphite tubes, (2) addition of chemical modifiers, (3) application of the mini-flow of the internal sheath gas, and (4) change of the graphite tube length. Moreover, a novel approach is offered for the interpretation of the irregular characteristics of the analytical curves.

Theoretical considerations

The initial idea of the present approach is that when the mass of the analyte changes in orders of magnitude range, the atomic vapour columns in the furnace may have different shape and size. An indirect proof for this follows from the mass dependent vaporization of analytes, as observed on a dissimilar appearance time (t_{app}) of the transient signals for varying analyte masses. This leads to diverse velocity profiles for the different amounts of samples during atomization (*i.e.* alternative sizes of the atomic cloud), since the greater analyte masses are evaporated in a temperature space with a faster expansion velocity, *i.e.* in a space with steeper temperature gradients, and pressure drops. Consequently, the loss of the analyte vapours could be different at the tube ends, and the greater loss is expected to occur at higher analyte amounts, *i.e.* at the upper parts of the calibration curves.

Under stationary heating of the THGA furnace, when no ramp is applied (*e.g.* at the end of a common pyrolysis stage, after interrupted internal gas flow), the static pressures in the furnace compartment are equal. When the furnace is heated with high heating rates (atomization step), the inner furnace gas expands together with the sample vapours. The dynamic heating causes differences in the temperatures, *i.e.* the outer parts of the gas phase around the tube is unable to follow closely the inner tube temperature, and also the expanding sheath gas and sample vapours increase the pressure differences between the tube ends and the furnace compartment (outer part of the tube). As an effect of these pressure gradients, a convection transport of the sheath gas and the sample vapours occurs in addition to diffusion. The average velocities (v_a) of the expelled atoms reached on dynamic heating can be calculated on the base of Holcombe's work.[23] For 2000 °C s^{-1} heating rate, the variation in v_a values at diverse t_{app} values of the transients (*e.g.* $\Delta t_{app} = 0.1$ s) exceeds 10% for the THGA tube ends, which is a remarkable discrepancy. The expulsion combined with diffusion and convection mass transport can cause the escape of analyte atoms from the optical path, which leads to the irregular characteristic of the calibration curves.

Experimental

Instrumentation

Two GFAAS instruments of the PerkinElmer Model SIMAA 6000 (Überlingen, Germany) installed in two different analytical laboratories of Hungary were employed for the experiments. Standard and end-capped designs of pyrolytically coated THGA tubes with integrated L'vov platform were used. In model experiments, a standard THGA tube was mechanically shortened by 0.5 mm at both ends, and cleaned out by several firings at 2450 °C. A Model AS-70 (PerkinElmer, Überlingen, Germany) autosampler was applied to deposit sample aliquots of 20 µl onto the platform. Hollow cathode lamps of Ag, Co, Cu, Cr, Mn, Mo, Ni and V were operated at the working currents recommended by the manufacturer.

Integrated absorbance (A_i) signals of Ag, Cr, Cu, Mo and V were measured at 328.1, 357.9, 324.8, 313.3 and 318.4 nm, respectively, with a spectral bandwidth (SW) of 0.7 nm. For Co, Mn and Ni, the 242.5, 279.5 and 232.0 nm lines were selected with a SW of 0.2 nm. The signal integration time was 3 s for Ag and Mn, 5 s for Co, Cr, Cu and Ni, and 7 s for Mo and V. High-purity (4N5) argon was used as a sheath gas. The data points of the calibration curves represent the average value of triplicate measurements (RSD < 4.7%). The absorbance data were corrected with the absorbance readings of the blank solutions. Detailed optimization procedures for simultaneous determinations can be found elsewhere.[4] The temperature program of the THGA furnace is listed in Table 1.

Table 1 Operating conditions for the THGA furnace

Step	Temperature/ °C	Ramp time/s	Hold time/s	Internal argon flow/cm^3 min^{-1}
Drying I	130	1	40	250
Drying II	200	10	20	250
Pyrolysis	Varied[a]	10	20	250
Atomization	Varied[b]	0[c]	5	0 or 50[d]
Clean-out	2450	1	3	250

[a]Pyrolysis temperature: 400 °C for Ag + Cu + Mn, 800 °C for Co + Cr + Cu, 700 °C for Co + Mn + Ni, and 1300 °C for Cr + Mo + V simultaneous determinations. [b]Atomization temperature: 2100 °C for Ag + Cu + Mn, 2300 °C for Co + Cr + Cu and for Co + Mn + Ni, and 2450 °C for Cr + Mo + V simultaneous determinations. [c]Maximum power heating (2300 °C s^{-1} for the THGA wall, corresponds to approximately 1000 °C s^{-1} for the integrated platform).[14] [d]Mini-flow conditions.

Data evaluation

As a first approach, the representative parameters of the calibration curves, *i.e.* the slope (S) and the correlation coefficient (R), were evaluated from linear fittings (least square method) to the calibration points. In order to estimate the correctness of the calibration curves, two criteria were utilized, as suggested by L'vov *et al.*[24] Firstly, the R value of the calibration should not be less than 0.9990. Secondly, the m_0 data, calculated from individual calibration points, should not deviate from the values recommended by the manufacturer. As a second approach, the linearity of the calibration curves was also assessed by applying second order fittings, *i.e.* using the equation: $A_i = a_0 + a_1c + a_2c^2$; where c is the concentration of the analyte, and a_0, a_1 and a_2 are the polynomial coefficients. The a_2 parameter is of dominant importance with respect to the linearity, *i.e.* the better of a_2 approaching to zero, the better the linearity of the calibration curve.

Reagents and methods

Multi-element calibration solutions were prepared from stock solutions, as described in detail in previous works.[2–4] Calibration graphs were also plotted with solutions, which were made with an appropriate dilution from standards of higher concentration. Using the autosampler 5, 10, or 15 µl sample volumes were dispensed, and some of the acidified diluents were added to obtain a total sample volume of 20 µl, *i.e.* the mixing of the calibration solution was done on the platform of the THGA tubes. As a comparison, the calibration solutions were also prepared by dilutions from a PerkinElmer "GFAAS Mixed Standard" (Überlingen, Germany) stock solution, which

contains 5 μg ml^{-1} Be and Cd, 10 μg ml^{-1} Ag, 20 μg ml^{-1} Cr, Fe, and Mn, 50 μg ml^{-1} Ba, Co, Cu, and Ni and 100 μg ml^{-1} Al, As, Pb, Sb, Se, and Tl, as certified concentration values.

In some experiments, either the mixture of 62.6 μg Bi_2TeO_5 plus 121.6 μg triammonium citrate (TAC) dissolved in 2.3% (m/v) HCl, or 5 μg $Pd(NO_3)_2$ plus 3 μg $Mg(NO_3)_2$ diluted from the PerkinElmer "Mixed Modifier" (Überlingen, Germany) solution, were applied as chemical modifiers. The Bi_2TeO_5 stock solution was made of the dissolution of high-purity Bi_2O_3 and TeO_2 in 6 M HCl. For the acidification and dilution of the solutions, Merck (Darmstadt, Germany) Suprapur grade acids, and ion-exchanged, doubly distilled water were used.

Results and discussion

Calibration curves of chromium

The calibration curves of Cr in the 0.5–50 μg l^{-1} concentration range are depicted in Fig. 1. When using standard THGA tubes and gas stop conditions during the atomization stage, the calibration points of Cr can be approached with two linear sections of different slopes (Fig. 1a, curve A). The higher slope belongs to the 0.5–5.0 μg l^{-1}, whereas the lower slope to the 5.0–50 μg l^{-1} concentration ranges. The ratio of the slopes was found to be 2.4, which is a remarkable discrepancy. Application of one linear fitting for the whole concentration range can introduce a large systematic error to the analytical results, which follows from the low correlation (R = 0.9940) of the linear and also the high a_2 value of the second order fittings (Table 2).

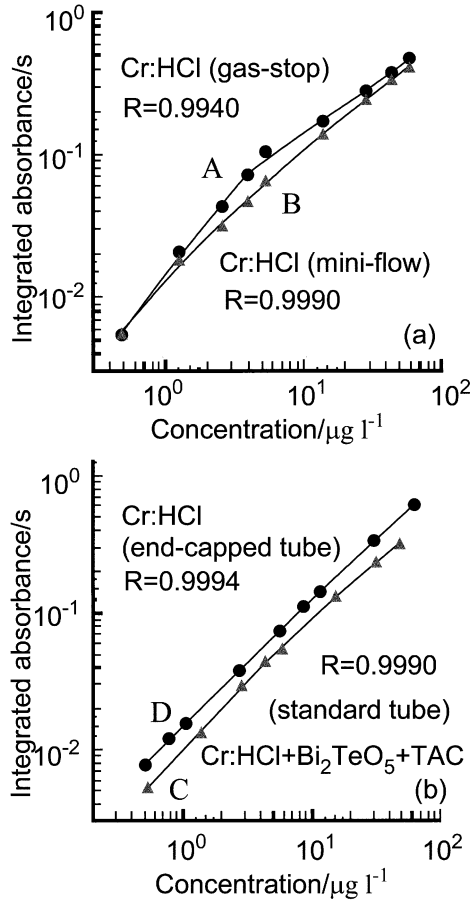

Fig. 1 Calibration curves of chromium in a multi-element (Mo, V) medium with 2.3% (m/v) HCl using standard THGA tubes under gas-stop (A), and mini-flow (50 cm^3 min^{-1}) of the internal sheath gas (B); with the addition of 62.6 μg Bi_2TeO_5 plus 121.6 μg triammonium citrate "TAC" chemical modifier under gas stop (C), and using end-capped THGA tubes under gas stop without modifier (D).

Table 2 Polynomial coefficients obtained from second order fittings to the calibration points of chromium and copper

	Polynomial coefficients		
Conditions	a_0	a_1	a_2
Chromium			
Gas stop	0.01385	1.3841	−0.1221
Mini-flow	0.01183	1.1356	−0.0521
Modifiers[a]	0.01122	1.1239	−0.0411
End-capped tube	0.01669	1.0349	−0.0135
Shortened tube	0.01313	1.0779	−0.0668
Copper			
Gas stop	0.00531	1.0539	−0.0282
Mini-flow	0.00391	0.9271	0.0148
Modifiers[b]	0.00335	1.0658	−0.0106
End-capped tube	0.00849	0.8834	0.0080
Shortened tube	0.00361	1.3298	−0.0175

[a]62.6 μg Bi_2TeO_5 plus 121.6 μg TAC. [b]5 μg $Pd(NO_3)_2$ plus 3 μg $Mg(NO_3)_2$.

Carrier gas flows applied during the atomization step allow the expansion of the dynamic range of the calibration, *e.g.* for Sn, half an order of magnitude increase in the linear range has been found.[25] Following this practice, the mini-flow condition of the internal sheath gas (50 cm^3 min^{-1}) was found to improve the linearity of the calibration (Fig. 1a, curve B). This can be experienced with better R (0.9990) and decreased a_2 values (Table 2), compared to those of found under gas stop. Mini-flow conditions produce a compressed velocity and concentration field of the thermal expansion within the furnace; *i.e.* the analyte vaporized, expands and expels towards the opened ends of the tube in a relatively shorter distance than under gas stop conditions. The important feature of mini-flow conditions that it likely results in a decreased role of expulsion, diffusion and natural convection losses at the tube ends. However, the sensitivity was dropped by a factor of 0.7 for Cr, due to the forced convection, which reduces the residence time of the sample vapours in the furnace.

Chemical modifiers are often applied in GFAAS to overcome a variety of interference effects.[26] In former works,[1–5] Bi_2TeO_5 matrix was successfully used as an "internal" modifier,[27] resulting in an enhancement on the Cr signal. The addition of 62.6 μg Bi_2TeO_5 plus 121.6 μg TAC (in HCl) to the Cr standards under gas stop conditions resulted in an improved linearity of calibration curves (Fig. 1b, curve C), *i.e.* better R (0.9990) and lower a_2 values of the fittings (Table 2).

As an alternative to the above methods, end-capped THGA tubes were applied under gas stop mode. This approach also resulted in linear calibration curves through more than two orders of magnitude in the whole dynamic range, with good correlation (R = 0.9994), as can be seen on Fig. 1b (curve D). The a_2 value was significantly decreased (Table 2), and exhibited the best value amongst the various methods studied. The effect of this tube design on the shape of the calibration curves can be interpreted on the base of the decreased loss of sample vapours at the tube ends, which is due to the presence of end-caps. Also a beneficial feature of the end-capped tubes is the prolonged residence time of sample vapours in the absorption volume, which results in a sensitivity enhancement of 1.7 for Cr, compared to that of standard THGA tubes.

Calibration curves of copper

The double sloping of the calibration curves of Cu were similar to that found for Cr, when using standard THGA tubes and gas stop conditions (Fig. 2a, curve A). According to the linear fitting (R = 0.9984), the higher slope belongs to the 1.0–2.5 μg l^{-1}, and the lower slope belongs to the 2.5–125 μg l^{-1}

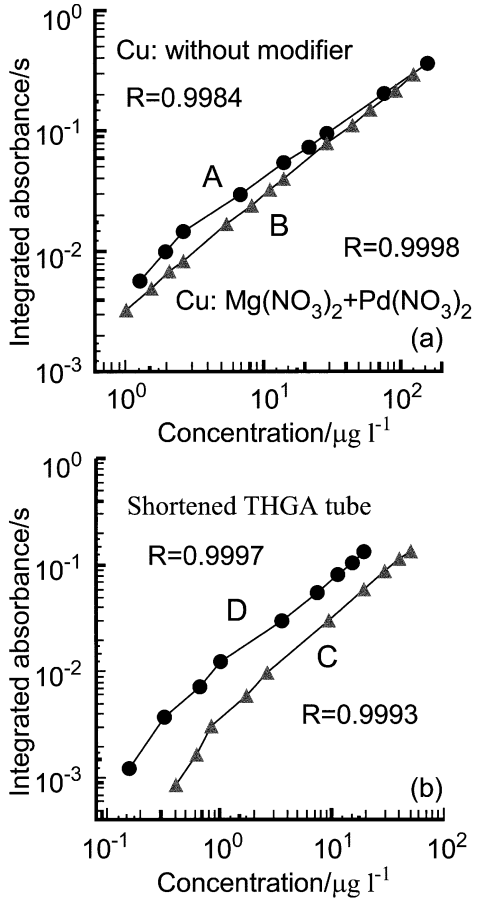

Fig. 2 Calibration curves of copper (A, B and C) and chromium (D) applied in 1.8% (m/v) nitric acid medium under gas stop conditions; without (A) and with the addition of 5 μg $Pd(NO_3)_2$ plus 3 μg $Mg(NO_3)_2$ chemical modifier (B), applying standard THGA tubes; and with a shortened standard THGA tube for Cu (C) and Cr (D).

concentration ranges. The ratio of the slopes was achieved to be 2.25, a similar value to that of Cr. The a_2 parameter was also found to be very high, showing a bad correlation. The three above methods, used for Cr, were also applicable to Cu, for realizing linear calibration curves in a broader concentration range. An example for this was the addition of Pd–Mg "mixed" chemical modifier to the standard solutions (Fig. 2a, curve B), resulting in an improved correlation of the linear fitting ($R = 0.9998$).

Other medium volatility elements, such as Ag, Co, Mn and Ni, were also studied, for which the irregular characteristics of the calibration curves were also observable, when measuring them in simultaneous, multi-element mode (see Table 6 later). However, the "double sloping" appeared to a less significant extent than for Cr and Cu.

Application of shortened THGA tubes

The calibration curves of Cr and Cu with shortened THGA tubes are depicted in Fig. 2b. Their irregular declination was more manifested and appeared at 1.0 and 0.9 μg l^{-1} for Cr and Cu, respectively; *i.e.* at lower concentrations, compared to standard THGA tubes (6.0 and 3.0 μg l^{-1} for Cr and Cu, respectively). Due to this effect, certainly, a better fitting of the calibration points was achieved with shortened tubes (Fig. 2b, Table 2), but at the expense of sensitivity decrease, even for the lower range of the calibration curves. Because of the shorter length of the furnace, a greater portion of the analyte atoms can reach the tube ends. Moreover, the enlarged gaps between the furnace housing and the tube ends likely results in an increased mass transport through the gaps. Consequently, it can be proposed that these gaps should be reduced to as small as possible, to minimize the vapour loss.

Calibration curves for molybdenum and vanadium

The calibration data for Mo and V from the simultaneous measurements of Cr, Mo and V are listed in Table 3. For these low volatile elements, single, linear calibration curves were found in the 1.0–100 and 5.0–400 μg l^{-1} concentration ranges, respectively. The R values showed good fittings of the curves to the calibration points, and also the m_0 data were in fairly good agreement with the data of the manufacturers, in the presence and absence of chemical modifiers as well.

Atomization transients

The absorbance–time curves of Cr are plotted in Fig. 3. When a standard solution of lower Cr concentration (1.3 μg l^{-1}) was applied under gas-stop conditions, the t_{app} was ~0.55 s, which decreased to ~0.43 s with the use of the solution of higher Cr content (13 μg l^{-1}). These t_{app} values were increased on the addition of chemical modifiers to around 1.0 and 0.85 s, respectively. Similarly, the time at peak height maximum (t_{peak}) was also shifted from 1.05 s to 1.26 s, not only on the addition of chemical modifiers, but using mini-flow conditions as well. In the presence of chemical modifiers, sharper and faster Cr transients can be observed (Fig. 3, curves C), which is due to a delayed vaporization of Cr, the vapour entering into a gas phase of higher and more homogeneous temperature.

The effect of dynamic heating was also studied on the simultaneous measurements of Cr and Cu by varying the pyrolysis temperature (T_{pyr}) at constant atomization temperature (T_{at}). It is expected from these experiments that the more lag exists between T_{pyr} and T_{at}, the steeper the temperature gradient appears along the longitudinal direction

Table 3 Analytical performance for Mo and V

	Gas stop		Mini-flow[4]/50 cm^3 min^{-1}	
	HCl[a]	HCl–Bi_2TeO_5–TAC[a]	HCl[a]	HCl–Bi_2TeO_5–TAC[a]
Molybdenum (1.0–100 μg l^{-1})				
S[b]/s l μg^{-1}	0.0069	0.0066	0.0046	0.0042
LOD[c]/μg l^{-1}	2.6	3.1	3.9	4.9
m_0[d]/pg	14.3	15.0	20.1	20.9
R[e]	0.9985	0.99995	0.9996	0.9995
Vanadium (5.0–400 μg l^{-1})				
S[b]/s l μg^{-1}	0.00197	0.00190	0.00134	0.0013
LOD[c]/μg l^{-1}	3.4	4.6	4.7	6.7
m_0[d]/pg	38.4	39.8	58.1	59.8
R[e]	0.9980	0.9992	0.9993	0.9996

[a]Concentrations: 2.3% (m/v) HCl, 62.6 μg Bi_2TeO_5, 121.6 μg triammonium citrate (TAC). [b]Slope of the calibration curve (linear fitting). [c]Limit of detection (3σ). [d]Characteristic mass. [e]Correlation coefficient of the linear fitting.

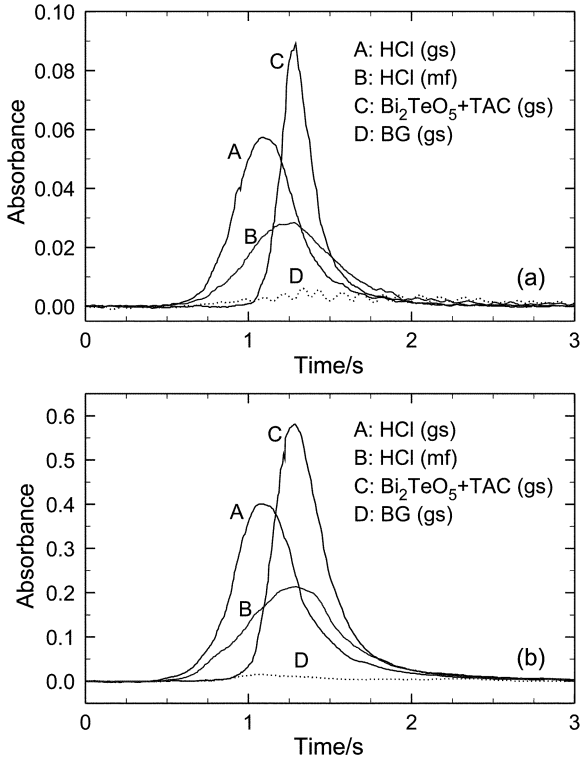

Fig. 3 Atomization transients of 26 pg (a) and 260 pg (b) chromium in a multi-element (Mo, V) medium with 2.3% (m/v) HCl, under gas-stop (curves A, C, D), and mini-flow "50 cm^3 min^{-1}" (curve B) conditions, without (A, B) and with 62.6 μg Bi_2TeO_5 plus 121.6 μg TAC chemical modifier (C, D)—standard THGA tubes are applied. Legends: (gs) gas stop and (mf) mini-flow, BG: background absorbance for blank solution.

of the furnace during atomization. This is a reasonable prospect on the basis of the temperature measurements of Sperling *et al.*[14] Consequently, the expulsion, diffusion and convection of the sample vapours could also become faster, which are expected to increase the loss. When decreasing T_{pyr}, *i.e.* rising the gap between T_{pyr} and T_{at}, a small, but significant increase has been found for the m_0 data of Cr and Cu at the upper part of the calibration graphs, which observation is in agreement with the expectations. As can be seen in Table 4, the increasing T_{pyr} decreased the t_{app} and t_{peak} values. The t_{app} data found with lower Cr and Cu standards were greater than those of the higher standard solutions. In addition, a significant increase of m_0 can be observed, when using standard solutions of higher analyte concentration (upper part of the calibration curves).

For Mo and V, the t_{app} and t_{peak} data were around 0.8 and 1.45 s, respectively, which values were increased on the addition of Bi_2TeO_5–TAC chemical modifier to 1.1 and 1.8 s, respectively, and further increased with the use of mini-flow conditions to 1.2 and 1.9 s, respectively. It is assumed that this delay in the vaporization is sufficient enough to reach steady state temperature conditions in the gas phase. On the contrary, when the medium volatile elements (such as Cr and Cu) are vaporized, the t_{app} is lower, 0.43 and 0.36 s, respectively, which time is too short to reach steady state conditions.[14] It is assumed that the lack of steady state conditions results in a more expressed decrease of the sensitivity at higher analyte concentrations, *i.e.* declining upper parts of the analytical curves.

Table 4 Appearance time (t_{app}) and time at peak height maximum (t_{peak}) of Cr and Cu transients with increasing pyrolysis temperature (T_{pyr}), under T_{at} = 2300 °C

	Cr		Cu	
Concentration/μg l^{-1}[a]	0.8	8.0	2.0	20.0
T_{pyr} = 400 °C				
t_{app}/s	0.87	0.75	0.61	0.56
t_{peak}/s	1.60	1.67	1.35	1.38
T_{pyr} = 800 °C				
t_{app}/s	0.63	0.53	0.45	0.39
t_{peak}/s	1.36	1.36	1.05	1.07
T_{pyr} = 1200 °C				
t_{app}/s	0.55	0.44	0.37	0.31
t_{peak}/s	1.24	1.20	0.98	0.95

[a]Standard solutions diluted from "GFAAS Mixed Standard".

Table 5 Diffusion coefficients of analyte atoms in argon at various atomization temperatures

	D_0 ($\times 10^{-6}$)[a]/ m^2 s^{-1}	n[b]	T_{at}/K	D ($\times 10^{-4}$)[c]/ m^2 s^{-1}
Ag	7.9	1.89	2170	3.98
			2370	4.71
Co	9.7	1.89	2570	6.73
Cr	10.3	1.88	2570	6.99
			2720	7.78
Cu	9.3	1.91	2370	5.78
			2570	6.75
Mn	13.0	1.70	2370	5.13
			2570	5.89
Ni	9.4	1.93	2570	7.14
Mo	9.1	1.88	2720	6.87
V	8.4	1.93	2720	7.11

[a]D_0: diffusion coefficient at 273 K.[28] [b]Gas combination factor.[28] [c]D: diffusion coefficient at the atomization temperature (T_{at}).

Comparison of the diffusivity data

Diffusion coefficients (D) of the analytes were calculated on the base of L'vov's data[28] (Table 5). The D values of Co, Cu, Cr, Ni, Mo and V are fairly high compared to those of Ag and Mn, under the present, optimized analytical conditions. For the former elements, the diffusion likely plays a more important role in the loss mechanism, as especially manifested in the shape of calibration curves for Cr and Cu. However, for Co, Ni, Mo and V, the vapour loss could be lesser, due to their quite greater t_{app} values (>0.7 s), even at higher analyte concentrations. Despite the short t_{app} of Ag and Mn, their lower D values exhibit lesser losses, *i.e.* a smaller irregularity of their calibration. It can be deduced that two criteria could be fulfilled to develop irregular calibration curves; firstly, a quite great D value of the analyte (>5.8 cm^2 s^{-1}), and secondly, a fairly short t_{app} of its transient (<0.6 s).

Evaluation of the analytical performance for various analyte combinations

The calibration data for various combinations of Ag, Co, Cu, Cr, Mn and Ni have shown a better linearity of the calibration curves under mini-flow conditions, compared to gas stop (Table 6). When mini-flow was used, the upper limit of the linear calibration range could be favourably extended by a factor of 1.5–2.0. Under this condition, the sensitivity drop on the slopes of Ag, Co, Cu, Cr, Mn and Ni was only 1.15–1.30 times lower than those of under gas stop, and also the LODs were negligibly increased, which are acceptable disadvantages.

In simultaneous, multi-element GFAAS, one has to apply compromise T_{pyr} and T_{at} settings,[18,29,30] which, due to the different volatility of the analytes, yields a wide temperature gap between the pyrolysis and atomization stages. Consequently, these conditions promote the appearance of greater temperature gradients, and pressure drops between the opened tube ends and the graphite furnace housing at the earlier stage of atomization. The higher gradients exhibit a greater internal sheath gas expansion, and also a greater expulsion,

Table 6 Calibration data of simultaneous, multi-element measurements for various sets of analytes

	Gas stop					Mini-flow (50 cm^3 min^{-1})				
	S^a/s l μg^{-1}	R^b	LOD^c/μg l^{-1}	C^d/μg l^{-1}	RSD (%)	S^a/s l μg^{-1}	R^b	LOD^c/μg l^{-1}	C^d/μg l^{-1}	RSD (%)
Ag	0.0155	0.9977	0.058	10	1.2–4.7	0.0124	0.9991	0.073	20	0.6–3.6
Cu	0.0052	0.9987	0.058	50	0.4–4.1	0.0044	0.9996	0.068	100	0.2–3.5
Mn	0.0174	0.9992	0.047	20	0.1–3.3	0.0134	0.9996	0.053	40	0.4–3.0
Co	0.0047	0.9990	0.190	50	0.1–2.3	0.0039	0.9998	0.240	100	0.2–3.1
Cr	0.0130	0.9898	0.046	40	0.2–3.1	0.0113	0.9991	0.053	60	0.2–2.0
Cu	0.0054	0.9986	0.048	50	0.1–1.7	0.0047	0.9995	0.061	100	0.2–1.5
Co	0.0043	0.9987	0.21	50	0.2–5.5	0.0034	0.9994	0.26	100	0.6–3.7
Mn	0.0151	0.9961	0.06	20	0.1–5.7	0.0116	0.9982	0.08	30	0.3–3.7
Ni	0.0034	0.9996	0.18	100	0.4–4.9	0.0029	0.9999	0.20	200	0.2–4.3

[a]Slope of the calibration curve (linear fitting). [b]Correlation coefficient. [c]Limit of detection (3σ). [d]Upper limit of the linear calibration curve.

diffusive (likely the main loss mechanism) and convective vapour transport of analyte atoms, *i.e.* a greater part of atoms reach the tube ends, and could escape from the optical path. These findings also present an alternative explanation for the irregular characteristic of the calibration curves for some low volatile elements, when using fast furnace programs; *i.e.* the maximum gap between pyrolysis and atomization temperatures.[9]

Conclusions

The irregular ''double sloping'' of the analytical curves is likely due to analyte vapour losses at the opened ends of the standard THGA tubes. The linearity of these curves can be improved by applying end-capped tubes, chemical modifiers, or mini-flow conditions, which favourable settings likely decrease the vapour loss associated with the tube ends.

It is also to be noted here, that the super-saturated matrix vapours can condense in the gas phase, and can cause a sensitivity decrease by removing the analyte atoms from the optical path, as trapped species, without atomization.[31] The investigation of these physical interference phenomena is, however, in the scope of another study. The magnetic field of the Zeeman BG corrector can also influence the shape of the calibration curves.[32,33] However, this absorbance range is well above that of studied in this work. Obviously, these effects were not taken into account throughout the present study.

The important conclusion of the present work is that the time-dependent temperature and concentration gradients between inside and outside of the THGA tube can have, in some exceptional cases, a serious impact on the shape of the calibration curves. This effect can be further intensified by the compromise furnace programs employed for the simultaneous determination of sample components of different volatility. In analytical practice, the selection of the similar volatile sample components is recommended for simultaneous measurements to prevent the appearance of steep gradients. For GFAAS modelling and analytical method elaborations all the above features have to be taken into account, which are valid for developing absolute atomic absorption spectroscopic detection as well.

Acknowledgements

The authors wish to express their gratitude to Professor Tibor Kántor (Loránd Eötvös University of Sciences) for his helpful advice and discussions on the preparation of this manuscript. The support from the Hungarian Scientific Research Fund (OTKA) was gratefully acknowledged under project numbers of T 029756 and F 042627.

References

1 Á. Péter, O. Szakács, I. Földvári, L. Bencs and F. A. Munoz, *Mater. Res. Bull.*, 1996, **31**, 1067–1073.
2 L. Bencs and O. Szakács, *Spectrochim. Acta, Part B*, 1997, **52**, 1483–1496.
3 L. Bencs, O. Szakács and T. Kántor, *Spectrochim. Acta, Part B*, 1999, **54**, 1193–1206.
4 L. Bencs, O. Szakács, T. Kántor, I. Varga and G. Bozsai, *Spectrochim. Acta, Part B*, 2000, **55**, 883–891.
5 O. Szakács, L. Bencs, T. Kántor, I. Varga and G. Bozsai, *Magy. Kem. Foly.*, 2002, **108**, 84–92.
6 W. Slavin, D. C. Manning and G. R. Carnrick, *At. Spectrosc.*, 1981, **2**, 137–145.
7 B. Radziuk, G. Rödel, H. Stenz, H. Becker-Ross and S. Florek, *J. Anal. At. Spectrom.*, 1995, **10**, 127–136.
8 B. Radziuk, G. Rödel, M. Zeiher, S. Mizuno and K. Yamamoto, *J. Anal. At. Spectrom.*, 1995, **10**, 415–422.
9 M. Hoenig and A. Cilissen, *Spectrochim. Acta, Part B*, 1997, **52**, 1443–1449.
10 A. Kh. Gilmutdinov, K. Yu. Nagulin and Y. A. Zakharov, *J. Anal. At. Spectrom.*, 1994, **9**, 643–650.
11 A. Kh. Gilmutdinov, B. Radziuk, M. Sperling, B. Welz and K. Yu. Nagulin, *Appl. Spectrosc.*, 1995, **49**, 413–424.
12 W. Frech, D. C. Baxter and B. Hütsch, *Anal. Chem.*, 1986, **58**, 1973–1977.
13 B. V. L'vov, *Inzh.-Fiz. Zh.*, 1959, **2**, 44–52, (in English: *Spectrochim. Acta, Part B*, 1984, **39**, 159–166).
14 M. Sperling, B. Welz, J. Hertzberg, C. Rieck and G. Marowsky, *Spectrochim. Acta, Part B*, 1996, **51**, 897–930.
15 W. Frech and B. V. L'vov, *Spectrochim. Acta,Part B*, 1993, **48**, 1371–1379.
16 N. Hadgu, K. E. A. Ohlsson and W. Frech, *Spectrochim. Acta,Part B*, 1996, **51**, 1081–1093.
17 G. Schlemmer, H. Schulze and C. Gönner, *Atomic Absorption Technical Summary*, No. TSAA-46 (B050-4288), PerkinElmer, Überlingen, Germany.
18 J. M. Harnly and B. Radziuk, *J. Anal. At. Spectrom.*, 1995, **10**, 197–206.
19 N. Hadgu and W. Frech, *Spectrochim. Acta, Part B*, 1997, **52**, 1431–1442.
20 N. Hadgu and W. Frech, *Spectrochim. Acta, Part B*, 1994, **49**, 445–457.
21 N. Hadgu, J. Gustafsson, W. Frech and O. Axner, *Spectrochim. Acta, Part B*, 1998, **53**, 923–943.
22 A. Kh. Gilmutdinov, T. M. Abdullina, S. F. Gorbachev and V. L. Makarov, *Spectrochim. Acta, Part B*, 1992, **47**, 1075–1092.
23 J. A. Holcombe, *Spectrochim. Acta, Part B*, 1983, **38**, 609–615.
24 B. V. L'vov, L. K. Polzik, A. V. Novichikhin, A. V. Borodin and A. O. Dyakov, *Spectrochim. Acta, Part B*, 1995, **50**, 1757–1768.
25 M. A. Bellara, M. Resano and J. R. Castillo, *Spectrochim. Acta, Part B*, 1997, **52**, 1223–1227.
26 D. L. Tsalev, V. I. Slaveykova and P. B. Mandjukov, *Spectrochim. Acta Rev.*, 1990, **13**, 225–274.
27 A. Hulanicki, E. Bulska, B. Godlewska and K. Wrobel, *Anal. Lett.*, 1989, **22**, 1341–1354.
28 B. V. L'vov, *Spectrochim. Acta, Part B*, 1990, **45**, 633–655.
29 J. M. Harnly and J. S. Kane, *Anal. Chem.*, 1984, **56**, 48–54.
30 M. Berglund, W. Frech and D. C. Baxter, *Spectrochim. Acta, Part B*, 1991, **46**, 1767–1777.
31 T. Kántor, *Spectrochim. Acta, Part B*, 1988, **43**, 1299–1320.
32 M. T. C. de Loos-Vollebregt, P. Van Oosten, M. J. De Koning and J. Podmos, *Spectrochim. Acta, Part B*, 1993, **48**, 1505–1515.
33 M. Berglund, W. Frech, D. C. Baxter and B. Radziuk, *Spectrochim. Acta, Part B*, 1993, **48**, 1381–1392.